Optically Active Defects at the SiC/SiO_2 Interface

B.C. Johnson,[1,*] J. Woerle,[2,3] D. Haasmann,[4] C.T.-K. Lew,[1] R.A. Parker,[1] H. Knowles,[5,6] B. Pingault,[5] M. Atature,[5] A. Gali,[7,8] S. Dimitrijev,[4] M. Camarda,[2,3] and J.C. McCallum[9]

[1] *Centre for Quantum Computing and Communication Technology, School of Physics, University of Melbourne, Melbourne, Victoria 3010, Australia*

[2] *Paul Scherrer Institut, 5232 Villigen, Switzerland*

[3] *Advanced Power Semiconductor Laboratory, ETH Zurich, Physikstrasse 3, 8092 Zurich, Switzerland*

[4] *Queensland Micro- and Nanotechnology Centre, Griffith University, Brisbane, Queensland 4111, Australia*

[5] *Atomic, Mesoscopic and Optical Physics Group, Cavendish Laboratory, University of Cambridge, Cambridge CB3 0HE, United Kingdom*

[6] *Department of Physics, Harvard University, Cambridge, Massachusetts 02138, USA*

[7] *Institute for Solid State Physics and Optics, Wigner Research Centre for Physics, Hungarian Academy of Sciences, PO. Box 49, Budapest, 1525, Hungary*

[8] *Department of Atomic Physics, Budapest University of Technology and Economics, Budafoki út 8, Budapest, 1111, Hungary*

[9] *School of Physics, University of Melbourne, Melbourne, Victoria 3010, Australia*

(Received 13 June 2019; revised manuscript received 6 August 2019; published 11 October 2019)

The SiC/SiO_2 interface is a central component of many SiC electronic devices. Defects intrinsic to this interface can have a profound effect on their operation and reliability. It is therefore crucial to both understand the nature of these defects and develop characterization methods to enable optimized SiC-based devices. Here we make use of confocal microscopy to address single SiC/SiO_2-related defects and show the technique to be a noncontact, nondestructive, spatially resolved and rapid means of assessing thequality of the SiC/SiO_2 interface. This is achieved by a systematic investigation of the defect density of the SiC/SiO_2 interface by varying the parameters of a nitric oxide passivation anneal after oxidation. Standard capacitance-based characterization techniques are used to benchmark optical emission rates and densities of the optically active SiC/SiO_2-related defects. Further insight into the nature of these defects is provided by low-temperature optical measurements on single defects.

DOI: 10.1103/PhysRevApplied.12.044024

I. INTRODUCTION

Silicon carbide (SiC) has attracted considerable attention for use in high-power, high-temperature, and high-frequency device applications [1,2]. As for silicon, a stable thermal oxide can be grown on the SiC surface, enabling the formation of metal-oxide-semiconductor (MOS) devices. However, despite considerable effort, the density of interface-related defects after standard thermal oxidation tends to be much higher than that found for the Si/SiO_2 interface [3–5]. These defects capture charge carriers in MOSFET channels, reducing the channel mobility (typically less than $20\,cm^2\,V^{-1}\,s^{-1}$) [6], and act as Coulombic scattering centers [7], impeding realization of the material's full potential.

The presence of both Si and C at the interface lends greater complexity to exact defect identification and the development of an efficient means to circumvent their detrimental effects. A range of characterization techniques have been used to assess interface quality. Paramagnetic Si and C dangling bonds have been identified by electron-paramagnetic-resonance measurements [8–10]. However, this defect, so important for understanding the Si/SiO_2 interface, is thought to play a minor role for SiC/SiO_2. Instead, electrically active traps consisting of sp^2-bonded or graphitic C clusters are thought to dominate interactions with charge carriers in SiC devices. These defects are readily assessed with capacitance-based electrical measurements. Furthermore, admittance-based measurements reveal a continuum of interface states in the band gap. Such measurements have been pivotal for providing a means to improve the SiC/SiO_2 interface quality. In addition, near-interface oxide traps (NIOTs) give rise to high densities of states around the conduction-band edge [7,11]. These defects are responsible for the threshold-shift instability. Early reports associated these traps with oxygen deficiency in SiO_2 [3,12]. However, subsequent theoretical studies proposed alternatives such as interstitial Si atoms

*johnsonb@unimelb.edu.au

and doubly bonded C—C dimers [13] or a Si_2—C—O structure, in which a CO unit substitutes an oxygen atom in a Si—O—Si bridge [14]. Experimental evidence further suggests that NIOTs consist of a number of different defects [15–17].

Various fabrication methods have been developed to reduce the density of these traps, the most-common being postoxidation annealing [18] and nitridation of the interface in nitric oxide (NO) or nitrous oxide (N_2O) ambients [19]. These methods have an affect on all defect types to various degrees. For the case of C clusters, nitridation results in their dissolution with a corresponding shift in the defect-energy-level position [20,21]. Photoluminescence (PL) has also been used extensively to characterize deep-level defects in bulk SiC. Recently, the optical properties of defects formed after oxidation near the SiC/SiO_2 interface were also investigated [22–31]. These defects can be addressed individually when an appropriate excitation wavelength is used. These defects have been integrated into electrical devices, indicating that they are in electrical communication with the SiC substrate [22,25], and optical structures [24] for possible quantum applications. These defects are associated with deep localized states in the band gap but their atomic structure remains unknown. These defects are the subject of the present work.

PL mapping has been extensively used to observe the spatial distribution of bulk defects [32–35] and their impact on the carrier lifetime [36,37]. It is clear that the spatial-imaging capabilities of optical microscopes and no specific need for device fabrication may offer key advantages over electrical techniques that are traditionally used to aid SiC/SiO_2-interface optimization. Thus far, no systematic study of the possible correlation between the optical and electrical properties of SiC/SiO_2-interface defects has been performed. We address this by using nitridation annealing techniques to passivate the interface states to various degrees. Passivation is found to have a significant impact on the optical properties of the interface defects. The trends correlate well with capacitance-based characterization, suggesting that PL mapping and especially confocal mapping may be used as a noncontact, nondestructive, spatially resolved means of assessing the quality of the SiC/SiO_2 interface.

II. METHODS

4*H*-SiC *n*-type epitaxial layers on *n*-type ⟨0001⟩ substrates are used to investigate optically and electrically active defects at the SiC/SiO_2 interface. Before oxidation the wafers are cleaned by a standard procedure consisting of a piranha solution (3:1 H_2SO_4:H_2O_2), HF, SC1 (5:1:1 H_2O:NH_3:H_2O_2), SC2 (6:1:1 H_2O:HCl:H_2O_2), and HF again. The oxidation parameters are systematically varied. First, samples are oxidized in dry O_2 at 1250°C and then annealed in a NO ambient for times up to 60 min at the same temperature. After surface preparation the back of the wafers is etched with HF and aluminum is immediately deposited with an electron-beam evaporator. Al depositions are performed through a shadow mask to produce 1-mm-diameter circular Al contacts on the oxidized SiC surfaces to form MOS capacitors. For an additional sample set, the Si and C faces of an *n*-type 4HSiC wafer (without an epitaxial layer so that the doping levels at each face are similar) are oxidized in dry O_2 at 800 °C for 10 min.

Room-temperature capacitance-voltage and conductance-voltage measurements are performed with a 1-kHz ac probe frequency (Andeen-Hagerling 2500A). A single value of the interface state density approximately at the midgap is determined by the Hill-Coleman method [38] and the flat-band voltage-shift instability after successive voltage cycles is measured simultaneously [7,11]. The capacitance in accumulation does not always clearly reach the oxide capacitance. Therefore, to determine the oxide thickness and the theoretical capacitance curve, the $\sqrt{d(1/C^2)/dV}$-versus-$1/C$ curve is extrapolated to the horizontal axis.

A schematic of the custom-built confocal microscope used for optical characterization is shown in Fig. 1 along with a typical confocal PL map of an oxidized SiC surface. This map shows the expected optically stable and very bright diffraction-limited spots associated with PL from single SiC/SiO_2-interface-related defects. The single-photon-emission properties of these defects are discussed elsewhere [22–25,27,29,30]. The microscope is equipped with a 532-nm continuous-wave laser,

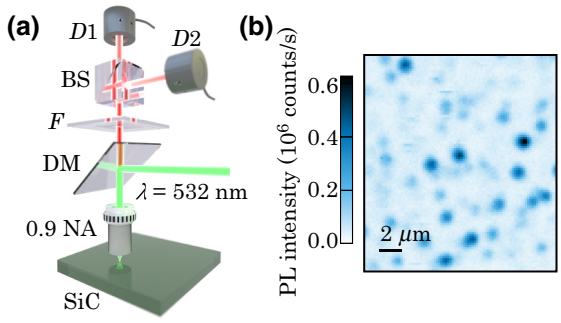

FIG. 1. (a) The custom-built confocal-imaging microscope showing the 532-nm laser directed onto a dichroic mirror (DM) via a fiber and reflected onto the sample, which is affixed to an *x*-*y*-*z* piezoelectric stage. PL from the sample is filtered by a filter (F) and collected through a fiber that acts as a confocal pinhole (CP) before being detected by a single-photon avalanche photodiode (D1). To assess whether the defect addressed is a single defect, a second detector (D2) may be used to form a Hanbury Brown–Twiss interferometer for single-photon-emission assessment. (b) A typical confocal image of the SiC/SiO_2 defects after a 30-min dry O_2 oxidation at 1100°C recorded with 1 mW of laser power before the objective. BS, beam splitter.

a dichroic mirror, a high-NA (0.95) 100× air objective, a 560-nm long-pass filter, and a fiber-coupled single-photon-counting module (PerkinElmer). The theoretical diffraction-limited spatial resolution of the technique is $0.44\lambda/(\mathrm{NA}) \approx 280$ nm [39] for emission wavelengths of 600 nm. All confocal images are collected at room temperature. For ensemble PL measurements of the SiC surface, we use a Renishaw inVia micro-Raman-spectrometer equipped with a 532-nm laser with a power on target of 10 mW in a spot approximately 10-μm in diameter. The exposure time for all PL spectra shown is 50 s.

III. RESULTS AND DISCUSSION

We first consider the difference between Si and C faces of 4*H*-SiC after oxidation at 800 °C for 10 min in O_2. This temperature is the lowest required to produce stable SiC/SiO_2-related-defect emission and corresponds to a few monolayers of SiO_2 (on the Si face) [40]. As a result, it is not possible to perform reliable electrical measurements on such ultrathin oxide layers without current leakage compromising the measurement. In contrast, SiC/SiO_2-related defects can be readily observed optically as shown in the PL confocal maps of these Si and C faces in Fig. 2(a). This illustrates one of the advantages of the optical technique to characterize defects where electrical contacts cannot be made.

The density of defects on the Si face is approximately 0.96×10^8 emitters/cm^2 as determined with an extensively tested image-analysis algorithm. Although the C-face sample is annealed simultaneously and has a similar surface roughness and doping density, the defect density is around an order of magnitude higher at approximately 1×10^9 emitters/cm^2. These defects are not completely resolved, and a much-brighter signal is obtained. A similar difference in defect density between the Si and C faces was identified by electrical measurements previously [41].

The defect densities quoted here are unique to the 532-nm-excitation maps. Each defect has a distinct PL spectrum with a zero-phonon line (ZPL) that appears in the 500–800-nm range [22,23]. The 532-nm laser does not excite all defects. A laser with a wavelength of less than 500 nm will excite a much-greater number of defects. Therefore, we estimate the actual defect density to be greater than an order of magnitude more dense than the values quoted above. This behavior is consistent with a broad band of defect states in the band gap rather than a discrete level common for a well-defined bulk defect. We further note that electrical measurements of the SiC/SiO_2-interface defects, as shown below, result in densities on the order of 10^{11} cm^{-2} eV^{-1}. However, the energy within the band gap over which the defects observed in Fig. 2 are addressed is not known. Therefore, a direct quantitative comparison is difficult at this stage.

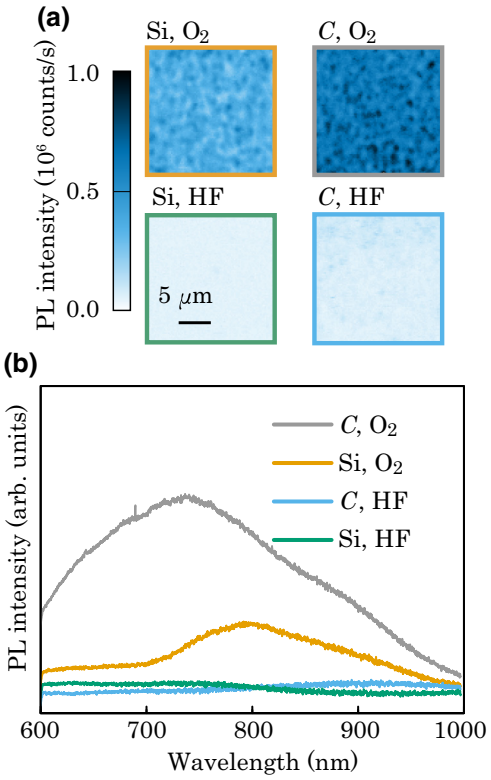

FIG. 2. (a) Confocal images (20 × 20 μm) of Si and C faces after oxidation at 800 °C for 10 min (top maps) and subsequent HF etching to remove the oxide (bottom maps). (b) The corresponding ensemble PL spectra for these samples.

After HF etching and removal of the SiO_2, the PL intensity and defect density are greatly reduced. For the Si face the defects are no longer observable. The C face retains a faint signal from the defects. We presume that HF is not as effective in removing the oxide on the C face as it is in removing it on the Si face. This may be a result of the differing chemistries of the two faces and requires further study. With the growth of a native oxide, optical defects again become visible, albeit with unstable intermittent photon emission.

The corresponding ensemble PL spectra are presented in Fig. 2(b). With a larger laser spot size, a greater number of interface defects are measured simultaneously. The oxidized C face clearly gives the most-intense PL, whereas the HF-etched surfaces give no appreciable signal. Again, when a shorter-wavelength laser is used, the broad PL signal becomes much more intense (not shown).

Figure 3 shows example PL spectra recorded at 4.2 K of these single SiC/SiO_2-related defects. The spectra are scaled to an energy relative to the ZPL position (i.e., the ZPL is at 0 meV). At these temperatures, the linewidth of the ZPL becomes extremely narrow (less than 0.2 nm) and the various components of the vibronic sideband, which arise from the electron-phonon interaction with intrinsic lattice phonons and local vibrations of the

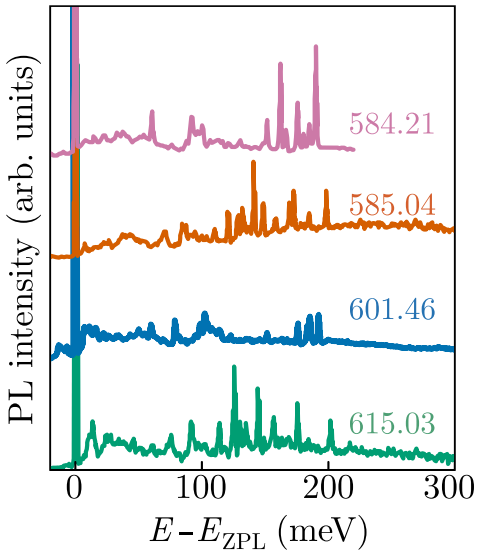

FIG. 3. PL spectra of single SiC/SiO_2 defects recorded at 4.2 K. The x-axis is the energy from the ZPL position of each defect. The ZPL position in nanometers is indicated next to each spectrum; the spectra are offset vertically for clarity.

defect center itself, can be clearly distinguished. As with the ZPL wavelength, each vibronic sideband shows great variability. Since the defect exists close to the SiC/SiO_2 interface, the vibronic sideband may consist of both SiC and SiO_2 intrinsic phonons and may further be subject to variations in the atomic structure of the defect. In general, there are some features common to each spectrum. Each consists of sharp high-energy local-vibration modes between 150 and 220 meV. These are greater in energy than the highest first-order Raman mode found in SiC (120 meV, or 960 cm^{-1}) and have energy ranges consistent with the vibrational modes of carbon and possibly oxygen-related bonds in SiC [26,42,43]. The source of the excess C is a by-product of the thermal-oxidation process and is known to make a considerable contribution to defects near or at the SiC/SiO_2 interface [3,44,45]. The number of local-vibration modes also varies but suggests that the defect is more complex than a simple point defect and may consist of a number of C—C or C—O bonds.

The ZPL energy, PL excited-state lifetime, and intensity of single defects as measured at 4.2 K are also found to be insensitive to magnetic fields up to 8 T along the c axis and up to 2 T along one of the a axes. This suggests that radiative recombination at these defects is likely to involve only singlet states. In addition, small jumps in the ZPL energy are occasionally observed, suggesting that the defect energy is sensitive to charge noise in the local environment.

For NO-passivated SiC/SiO_2, a series of capacitance and conductance electrical measurements are presented in Fig. 4. The bias sweep direction is toward inversion, while the starting voltage is incrementally increased toward accumulation. This allows quantification of the charge instability, which arises from NIOT defects close to the conduction-band edge. This is observed in a flat-band-voltage shift (ΔV_{FB}, taken to be the change in the point of inflection of the C-V curves). For MOS capacitors formed without a NO-passivation anneal, large shifts in the flat-band voltage are observable. The density of NIOTs is proportional to ΔV_{FB} divided by the change in the corresponding surface potential, $\Delta\psi_s$, determined with a simulated high-frequency C-V curve ($\Delta V_{\mathrm{FB}}/\Delta\psi_s \times C_{\mathrm{ox}}/\mathrm{qA}$). The C-V curve is calculated following the method outlined in Ref. [46].

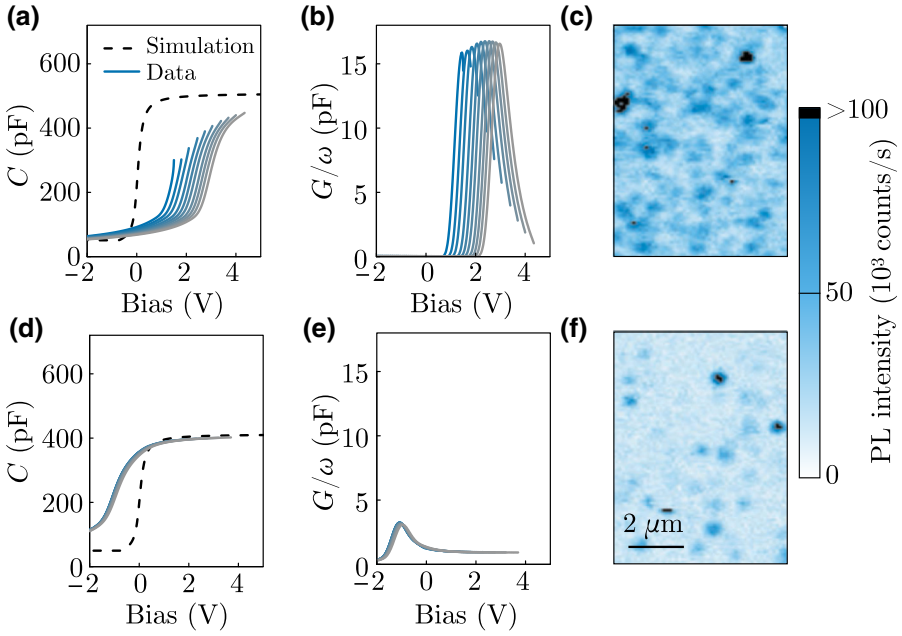

FIG. 4. Capacitance and conductance of SiC MOS capacitors fabricated (a),(b) without and (d),(e) with a NO-passivation anneal for a duration of 60 min. These oxides have thicknesses of 36 and 44 nm, respectively. The sweep direction is toward inversion, with initial voltages that progressively increase toward accumulation. For clarity only a few C-V and G-V traces are shown from the complete data set. The theoretical high-frequency capacitance trace with which the surface potential is determined is also shown (dashed line). (c),(f) The corresponding confocal maps of the SiC/SiO_2 surfaces without and with a NO anneal, respectively.

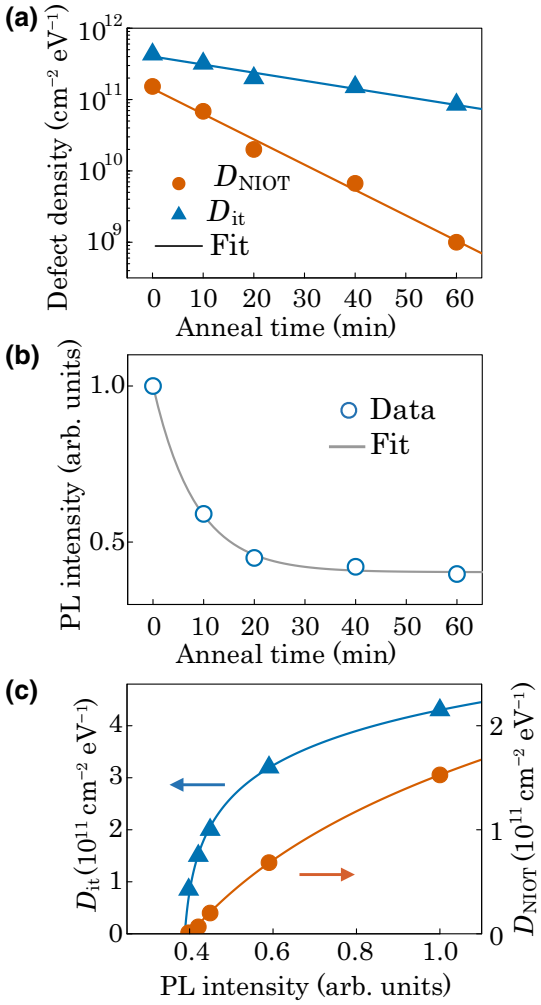

FIG. 5. (a) D_{it} and D_{NIOT} values extracted from C-V measurements like those shown in Fig. 4 as a function of the duration of the NO anneal. (b) The integrated PL intensity for the same samples. (c) The integrated PL intensity versus D_{it} and D_{NIOT}. The fitted exponential curves are guides for the eye. Note the difference in the scales of the left and right axes in (c).

For the oxide without a passivation anneal, $D_{NIOT} = 1.5 \times 10^{11}$ cm^{-2} eV^{-1} around the conduction-band edge is determined from the data presented in Fig. 4(a). Further details on the calculation are described in Ref. [11]. The corresponding conductance, measured simultaneously and corrected for series resistance [46], is shown in Fig. 4(b), where the peak height of conductance is proportional to the interface trap density $D_{it} = 4.3 \times 10^{11}$ cm^{-2} eV^{-1}. With a 60-min NO postoxidation anneal the defect-related signals are dramatically reduced, with densities of $D_{NIOT} = 1 \times 10^{9}$ cm^{-2} eV^{-1} and $D_{it} = 8.5 \times 10^{10}$ cm^{-2} eV^{-1}. That is, by a factor of 150 and 5 for D_{NIOT} and D_{it}, respectively. We note a slight increase in D_{it} as the measurement progresses. This behavior is common in all devices measured.

These results agree well with previous findings where nitridation is found to reduce the interface defect density by almost an order of magnitude [47]. The mechanism is a result of the trapping of N at the SiC/SiO_2 interface, where it is thought to directly passivate the C atoms in C clusters. The passivated component introduces a level near the valence band, while the trap energy associated with the cluster is reduced as a consequence of being proportional to its size [48].

The corresponding confocal images of these NO-passivated SiC/SiO_2 devices are shown in Figs. 4(c) and 4(f) as recorded on the Si face between the Al contacts. These images are similar to the image shown in Fig. 1(b) in that they show an array of bright defects as expected for an oxidized-Si-face SiC surface. The impact of the NO anneal can be seen in both the reduction in the emitter density and the emission rates in the confocal maps. The density for the sample without the NO anneal is similar to that in Figs. 1(b) and 2(a) at approximately 1×10^{8} emitters/cm^{2}. After the NO anneal, less than half the emitters remain. The intensity of these emitters is also reduced.

We find that the integrated intensity of these maps, or equivalently of the ensemble PL intensity, is a convenient gauge of the interface quality. As nitridation results in the dissolution of C clusters with a corresponding shift in energy-level position of the defect state in the band gap and, presumably the Fermi-level energy, we may describe this decrease in PL intensity as a modification of the recombination rate at the defect (Shockley-Reed-Hall recombination rate at a deep level) or the appearance of competing nonradiative recombination pathways.

We summarize the defect densities as a function of the anneal time in Fig. 5. Both D_{it} and D_{NIOT} decrease exponentially with time constants of 38.3 and 12.2 min, respectively, over the anneal-duration range considered. The integrated PL of the corresponding confocal maps is shown in Fig. 5(b). Initially, the PL decreases with a time constant of 10.9 min but starts to asymptote once it has dropped to 40% of the initial value. That is, NO anneals longer than 20 min do not appear to be as effective in further reducing the density of optically active defects. This is further highlighted in Fig. 5(c), where a saturation-type behavior is apparent when D_{it} and D_{NIOT} are plotted against the PL intensities, particularly, for $D_{it} < 3 \times 10^{11}$ cm^{-2} eV^{-1}. As D_{it} and D_{NIOT} show different behavior, we suggest that the origin of the optical defects may be distinct yet can still be used as a measure of interface quality over a fairly broad range of oxidation conditions.

IV. CONCLUSION

We investigate the utility of SiC/SiO_2-interface-related optical defects as an indicator of interface quality, a parameter of central importance for the realization of SiC devices. We find that the defect densities determined by both optical and electrical means are reduced by an increase in the duration of the NO anneal. The optical measurements show that both the density and the emission

rates of the defects are reduced by the NO anneal, due to passivation and a change in the recombination kinetics, respectively. This reduction is also observed for D_{it} and D_{NIOT} measured via capacitance measurements. The relationship between the PL intensity and these defect densities is found to have a saturation-type behavior since the PL intensity does not tend to reduce below 40% of its initial value.

Single-defect spectroscopy allows us to ascertain the properties of SiC/SiO_2-interface-related optical defects that would otherwise be obscured by their great variability. This can be used to great advantage to provide valuable information about the possible atomic origin of these defects as demonstrated in the low-temperature measurements presented in Fig. 3. Despite the large changes in density and spectral characteristics demonstrated here, we believe it reasonable to assume that all optically active defects associated with the SiC/SiO_2 interface belong to a single defect family. This is mainly due to the common circumstances under which they are formed, their common recombination kinetics, and there being no convincing evidence to the contrary as yet. We further stress that this variability demands a statistical approach. We achieve this here by ensemble PL measurements [with a large excitation volume; see Fig. 2(b)] or by integrating the total intensity of a confocal PL map [Fig. 5(b)]. This is an essential step in comparing the optical and electrical properties of the SiC/SiO_2-related defects. These methods are transferable to the C face, other SiC polytypes, and oxide growth processes.

ACKNOWLEDGMENTS

This research was funded by the Australian Research Council Centre of Excellence for Quantum Computation and Communication Technology (Grant No. CE170100012). A.G. is supported by the National Research Development and Innovation Office of Hungary (Grant No. 127902) and the Quantum Technology National Excellence Program (Project No. 2017-1.2.1-NKP-2017-00001).

[1] H. Matsunami, Technological breakthroughs in growth control of silicon carbide for high power electronic devices, Jpn. J. Appl. Phys. **43**, 6835 (2004).

[2] Gang Liu, Blair R. Tuttle, and Sarit Dhar, Silicon carbide: A unique platform for metal-oxide-semiconductor physics, Appl. Phys. Rev. **2**, 021307 (2015).

[3] V. V. Afanas'ev, M. Bassler, G. Pensl, and M. Schulz, Intrinsic SiC/SiO_2 interface states, Phys. Status Solidi A **162**, 321 (1997).

[4] S. Harada, R. Kosugi, J. Senzaki, W. J. Cho, K. Fukuda, K. Arai, and S. Suzuki, Relationship between channel mobility and interface state density in SiC metal–oxide–semiconductor field-effect transistor, J. Appl. Phys. **91**, 1568 (2002).

[5] A. J. Lelis, R. Green, D. B. Habersat, and M. El, Basic mechanisms of threshold-voltage instability and implications for reliability testing of SiC MOSFETs, IEEE Trans. Electron Devices **62**, 316 (2015).

[6] R. Schomer, P. Friedrichs, D. Peters, and D. Stephani, Significantly improved performance of MOSFETs on silicon carbide using the 15R-SiC polytype, IEEE Electron Device Lett. **20**, 241 (1999).

[7] Dai Okamoto, Hiroshi Yano, Yuki Oshiro, Tomoaki Hatayama, Yukiharu Uraoka, and Takashi Fuyuki, Investigation of near-interface traps generated by NO direct oxidation in C-face 4H-SiC metal–oxide–semiconductor structures, Appl. Phys. Express **2**, 021201 (2009).

[8] J. L. Cantin, H. J. von Bardeleben, Y. Shishkin, Y. Ke, R. P. Devaty, and W. J. Choyke, Identification of the Carbon Dangling Bond Center at the $4H-SiC/SiO_2$ Interface by an epr Study in Oxidized Porous SiC, Phys. Rev. Lett. **92**, 015502 (2004).

[9] P. J. Macfarlane and M. E. Zvanut, Characterization of paramagnetic defect centers in three poly types of dry heat treated, oxidized SiC, J. Appl. Phys. **88**, 4122 (2000).

[10] David J. Meyer, Patrick M. Lenahan, and Aivars J. Lelis, Observation of trapping defects in 4H-silicon carbide metal-oxide-semiconductor field-effect transistors by spin-dependent recombination, Appl. Phys. Lett. **86**, 023503 (2005).

[11] Hamid Amini Moghadam, Sima Dimitrijev, Ji Sheng Han, Amirhossein Aminbeidokhti, and Daniel Haasmann, in *Silicon Carbide and Related Materials 2015*, Materials Science Forum Vol. 858 (Trans Tech Publications, 2016), p. 603.

[12] V. V. Afanas'ev, A. Stesmans, M. Bassler, G. Pensl, and M. J. Schulz, Shallow electron traps at the $4H-SiC/SiO_2$ interface, Appl. Phys. Lett. **76**, 336 (2000).

[13] Jan M. Knaup, Peter Deák, Thomas Frauenheim, Adam Gali, Zoltán Hajnal, and W. J. Choyke, Theoretical study of the mechanism of dry oxidation of 4H-SiC, Phys. Rev. B **71**, 235321 (2005).

[14] F. Devynck, A. Alkauskas, P. Broqvist, and A. Pasquarello, Charge transition levels of carbon-, oxygen-, and hydrogen-related defects at the SiC/SiO_2 interface through hybrid functionals, Phys. Rev. B **84**, 235320 (2011).

[15] H.Ö. Ólafsson, Einar Ö. Sveinbjörnsson, T. E. Rudenko, V. I. Kilchytska, I. P. Tyagulski, and I. N. Osiyuk, A study of the shallow electron traps at the $4H-SiC/SiO_2$ interface, Mater. Sci. Forum **433**, 547 (2003).

[16] X. D. Chen, S. Dhar, T. Isaacs-Smith, J. R. Williams, L. C. Feldman, and P. M. Mooney, Electron capture and emission properties of interface states in thermally oxidized and NO-annealed $SiO_2/4H-SiC$, J. Appl. Phys. **103**, 033701 (2008).

[17] S. Dhar, X. D. Chen, P. M. Mooney, J. R. Williams, and L. C. Feldman, Ultrashallow defect states at $SiO_2/4H-SiC$ interfaces, Appl. Phys. Lett. **92**, 102112 (2008).

[18] L. A. Lipkin and J. W. Palmour, Improved oxidation procedures for reduced SiO_2/SiC defects, J. Electron. Mater. **25**, 909 (1996).

[19] H. Li, S. Dimitrijev, H. B. Harrison, and D. Sweatman, Interfacial characteristics of N_2O and NO nitrided SiO_2 grown on SiC by rapid thermal processing, Appl. Phys. Lett. **70**, 2028 (1997).

[20] K.-C. Chang, L. M. Porter, J. Bentley, C.-Y. Lu, and J. Cooper, Electrical, structural, and chemical analysis of silicon carbide-based metal-oxide-semiconductor field-effect-transistors, J. Appl. Phys. **95**, 8252 (2004).

[21] P. Jamet, S. Dimitrijev, and P. Tanner, Effects of nitridation in gate oxides grown on 4H-SiC, J. Appl. Phys. **90**, 5058 (2001).

[22] A. Lohrmann, N. Iwamoto, Z. Bodrog, S. Castelletto, T. Ohshima, T. J. Karle, A. Gali, S. Prawer, J. C. McCallum, and B. C. Johnson, Single-photon emitting diode in silicon carbide, Nat. Comms. **6**, 7783 (2015).

[23] A. Lohrmann, S. Castelletto, J. R. Klein, T. Ohshima, M. Bosi, M. Negri, D. W. M. Lau, B. C. Gibson, S. Prawer, J. C. McCallum, and B. C. Johnson, Activation and control of visible single defects in 4H-, 6H-, and 3C-SiC by oxidation, Appl. Phys. Lett. **108**, 021107 (2016).

[24] Alexander Lohrmann, Timothy James Karle, Vikas Kanayalal Sewani, Arne Laucht, Matteo Bosi, Marco Negri, Stefania Castelletto, Steven Prawer, Jeffrey Colin McCallum, and Brett Cameron Johnson, Integration of single-photon emitters into 3C-SiC microdisk resonators, ACS Photonics **4**, 462 (2017).

[25] Matthias Widmann, Matthias Niethammer, Takahiro Makino, Torsten Rendler, Stefan Lasse, Takeshi Ohshima, Jawad Ul Hassan, Nguyen Tien Son, Sang-Yun Lee, and Jörg Wrachtrup, Bright single photon sources in lateral silicon carbide light emitting diodes, Appl. Phys. Lett. **112**, 231103 (2018).

[26] Y. Abe, T. Umeda, M. Okamoto, R. Kosugi, S. Harada, M. Haruyama, W. Kada, O. Hanaizumi, S. Onoda, and T. Ohshima, Single photon sources in 4H-SiC metal-oxide-semiconductor field-effect transistors, Appl. Phys. Lett. **112**, 031105 (2018).

[27] Shin-Ichiro Sato, Tomoya Honda, Takahiro Makino, Yasuto Hijikata, Sang-Yun Lee, and Takeshi Ohshima, Room temperature electrical control of single photon sources at 4H-SiC surface, ACS Photonics **5**, 3159 (2018).

[28] Yasuto Hijikata, Takashi Horii, Yoritaka Furukawa, Yu-ichiro Matsushita, and Takeshi Ohshima, Oxygen-incorporated single-photon sources observed at the surface of silicon carbide crystals, J. Phys. Comm. **2**, 111003 (2018).

[29] Yuta Abe, Takahide Umeda, Mitsuo Okamoto, Shinobu Onoda, Moriyoshi Haruyama, Wataru Kada, Osamu Hanaizumi, Ryoji Kosugi, Shinsuke Harada, and Takeshi Ohshima, in *Silicon Carbide and Related Materials 2017*, Materials Science Forum Vol. 924 (Trans Tech Publications, 2018), p. 281.

[30] Hiroki Tsunemi, Tomoya Honda, Takahiro Makino, Shinobu Onoda, Shinichiro Sato, Yasuto Hijikata, and Takeshi Ohshima, in *Silicon Carbide and Related Materials 2017*, Materials Science Forum Vol. 924 (Trans Tech Publications, 2018), p. 204.

[31] Judith Woerle, Brett C. Johnson, Corrado Bongiorno, Kohei Yamasue, Gabriel Ferro, Dipanwita Dutta, Thomas A. Jung, Hans Sigg, Yasuo Cho, Ulrike Grossner, and Massimo Camarda, Two-dimensional defect mapping of the SiO_2/4H-SiC interface, Phys. Rev. Mater. **3**, 084602 (2019).

[32] J. M. Bluet, L. Masarotto, I. El Harrouni, and G. Guillot, UV scanning photoluminescencespectroscopy applied to silicon carbide characterisation, Mater. Sci. Eng. B **102**, 277 (2003).

[33] M. Tajima, E. Higashi, T. Hayashi, H. Kinoshita, and H. Shiomi, Nondestructive characterization of dislocations and micropipes in high-resistivity 6H-SiC wafers by deep-level photoluminescence mapping, Appl. Phys. Lett. **86**, 061914 (2005).

[34] Yutaro Miyano, Ryosuke Asafuji, Shuhei Yagi, Yasuto Hijikata, and Hiroyuki Yaguchi, Photoluminescence study of oxidation-induced faults in 4H-SiC epilayers, AIP Adv. **5**, 127116 (2015).

[35] Radu Hristu, Stefan G. Stanciu, Denis E. Tranca, Efstathios K. Polychroniadis, and George A. Stanciu, Identification of stacking faults in silicon carbide by polarization-resolved second harmonic generation microscopy, Sci. Rep. **7**, 4870 (2017).

[36] Tetsuya Miyazawa, Masahiko Ito, and Hidekazu Tsuchida, Evaluation of long carrier lifetimes in thick 4H silicon carbide epitaxial layers, Appl. Phys. Lett. **97**, 202106 (2010).

[37] P. B. Klein, B. V. Shanabrook, S. W. Huh, A. Y. Polyakov, M. Skowronski, J. J. Sumakeris, and M. J. O'Loughlin, Lifetime-limiting defects in n 4H-SiC epilayers, Appl. Phys. Lett. **88**, 052110 (2006).

[38] W. A. Hill and C. C. Coleman, A single-frequency approximation for interface-state density determination, Solid-State Electron. **23**, 987 (1980).

[39] Robert H. Webb, Confocal optical microscopy, Rep. Prog. Phys. **59**, 427 (1996).

[40] Y. Hijikata, H. Yaguchi, S. Yoshida, and S. Yagi, *Physics and Technology of Silicon Carbide Devices*, edited by Y. Hijikata (InTech, Croatia, 2013), Vol. 7.

[41] S. Dhar, L. C. Feldman, S. Wang, T. Isaacs-Smith, and J. R. Williams, Interface trap passivation for SiO_2/(0001) C-terminated 4H-SiC, J. Appl. Phys. **98**, 014902 (2005).

[42] A. Gali, P. Deák, P. Ordejón, N. T. Son, E. Janzén, and W. J. Choyke, Aggregation of carbon interstitials in silicon carbide: A theoretical study, Phys. Rev. B **68**, 125201 (2003).

[43] Alexander Mattausch, Michel Bockstedte, and Oleg Pankratov, Structure and vibrational spectra of carbon clusters in SiC, Phys. Rev. B **70**, 235211 (2004).

[44] E. Pippel, J. Woltersdorf, H. O. Olafsson, and E. O. Sveinbjornsson, Interfaces between 4H-SiC and SiO_2: Microstructure, nanochemistry, and near-interface traps, J. Appl. Phys. **97**, 034302 (2005).

[45] M. Bassler, G. Pensl, and V. Afanas'ev, "Carbon cluster model" forelectronic states at SiC/SiO_2 interfaces, Diamond Relat. Mater. **6**, 1472 (1997).

[46] E. H. Nicollian and J. R. Brews, *MOS (Metal Oxide Semi Conductor) Physics and Technology* (Wiley and Sons, New York, 1982).

[47] G. Y. Chung, C. C. Tin, J. R. Williams, K. McDonald, M. Di Ventra, S. T. Pantelides, L. C. Feldman, and R. A. Weller, Effect of nitric oxide annealing on the interface trap densities near the band edges in the 4H polytype of silicon carbide, Appl. Phys. Lett. **76**, 1713 (2000).

[48] K. McDonald, R. A. Weller, S. T. Pantelides, L. C. Feldman, G. Y. Chung, C. C. Tin, and J. R. Williams, Characterization and modeling of the nitrogen passivation of interface traps in SiO_2/4H-SiC, J. Appl. Phys. **93**, 2719 (2003).